

GODDARD
GRANT

IN-43-CR

161098

P-47

USE OF LANDSAT IMAGES OF VEGETATION COVER
TO ESTIMATE EFFECTIVE HYDRAULIC PROPERTIES OF SOILS

Peter S. Eagleson
Principal Investigator

and

Michael F. Jasinski
Research Assistant

Department of Civil Engineering
Massachusetts Institute of Technology
Cambridge, Massachusetts 02139

Final Technical Report

NAG 5 - 510

1 August 1988

(NASA-CR-183185) USE OF LANDSAT IMAGES OF VEGETATION COVER TO ESTIMATE EFFECTIVE HYDRAULIC PROPERTIES OF SOILS Final Technical Report (Massachusetts Inst. of Tech.) 47 p

N88-28514

Unclas
CSCL 02C G3/43 0161098

Final Technical Report

on

NAG 5 - 510

The work has focused on the characterization of natural, spatially variable, semivegetated landscapes using a linear, stochastic, canopy-soil reflectance model. A first application of the model was the investigation of the effects of subpixel and regional variability of scenes on the shape and structure of red-infrared scattergrams (See appended report, Jasinski and Eagleson, 1988). Additionally, the model was used to investigate the inverse problem, the estimation of subpixel vegetation cover, given only the scattergrams of simulated satellite scale multispectral scenes. The major aspects of that work, including recent field investigations, are summarized below.

Theoretical Analyses. In many natural, semivegetated landscapes, modeling reflected radiation in the visible and near infrared regions is difficult due to the highly random nature of many subpixel scale properties of the plant (e.g. plant geometry, leaf area, shape and orientations) and the soil (e.g. surface roughness, texture, moisture content, and organic matter content). In order to accommodate the random subpixel fluctuations, yet keep the number of model parameters to a minimum, Jasinski and Eagleson (1988) modeled the semivegetated landscape using a geometric canopy-soil reflectance model with random variables. The overall approach was to retain the bulk plant and soil parameters which dominate scene reflectance, such as fractional cover, plant geometry, plant and soil reflectance, and shadows, but to absorb the numerous secondary parameters contributing to subpixel variability into random reflectance terms. Such an approach is consistent with mesoscale hydrologic investigations which require primarily the bulk scene parameters for computing surface moisture and heat fluxes.

PRECEDING PAGE BLANK NOT FILMED

The canopy-soil reflectance model was used to interpret the information content of red-infrared scattergrams in terms of the physical structure of the scene. That was achieved by the sequential introduction of each variable into the scene, and observing its effect on the scattergram. In particular, the principal mechanisms which contribute to the often observed triangular shape, or "tasseled cap" were identified, including variable vegetation density, shadows, and variable soil background reflectance. The importance of the pixel scale relative to the scale of the plant and plant shadows was discussed. The results of that work are detailed in the appended report.

Recently, it has been demonstrated that the fractional (i.e. subpixel) vegetation cover of the simulated scenes can be retrieved by applying the method of moments to the aggregated scene. The method consists of equating the theoretical moments of the canopy-soil reflectance to the actual moments of the scene, and then solving for the unknown variables. At least seven moment equations can be written for the reflectance model, including five reflectance moments (i.e., the mean and variance of the reflectance equation in the red and infrared bands, and the cross-covariance) and two cover moments (i.e., the mean and variance). Conditional moments can also be written through the a priori understanding of the structure of the red-infrared scattergram. For instance, the means and variances of the soil reflectance terms can be written for the locus of pixels which constitute the soil line.

The inverse problem was applied to two test cases. For the Case II simulation (referred to in the appended report), the fractional vegetation cover was estimated by writing conditional moment equations along lines parallel to the soil line, as shown in the scattergram in Figure 1. For the Case V simulation, the analysis includes the writing of conditional moments for statistically homogeneous areas as shown in Figure 2. Comparisons of the estimated and actual mean vegetation cover for a range of cover types are provided in Figures 3 and 4, respectively. Results

indicate very good agreement. Details of these results are currently being summarized for publication in an appropriate journal.

The stochastic canopy-soil reflectance model has also provided a mechanism for studying the influence of scene variability on common vegetation indices, such as the normalized vegetation index (NVI). One important conclusion of that study is that the maximum NVI of a scene does not necessarily represent maximum vegetation amount, but it is affected by both shadows and soil variability. A third journal article detailing those results will be completed shortly.

Field Work. Work has included the application of the theoretical techniques developed above to actual aerial and satellite multispectral data. Two sets of aerial multispectral data were obtained during the month of June, 1988. The first data set was obtained over the Maricopa Agricultural Research Center, Arizona, as part of a larger experiment coordinated by the U.S.D.A. Water Conservation Lab, Phoenix. A second data set was conducted over three specified watersheds in the Beaver Creek Basin of the Coconino National Forest in northern Arizona. Also, Landsat Thematic Mapper Scenes of both areas are being acquired in order to test the model on actual satellite data.

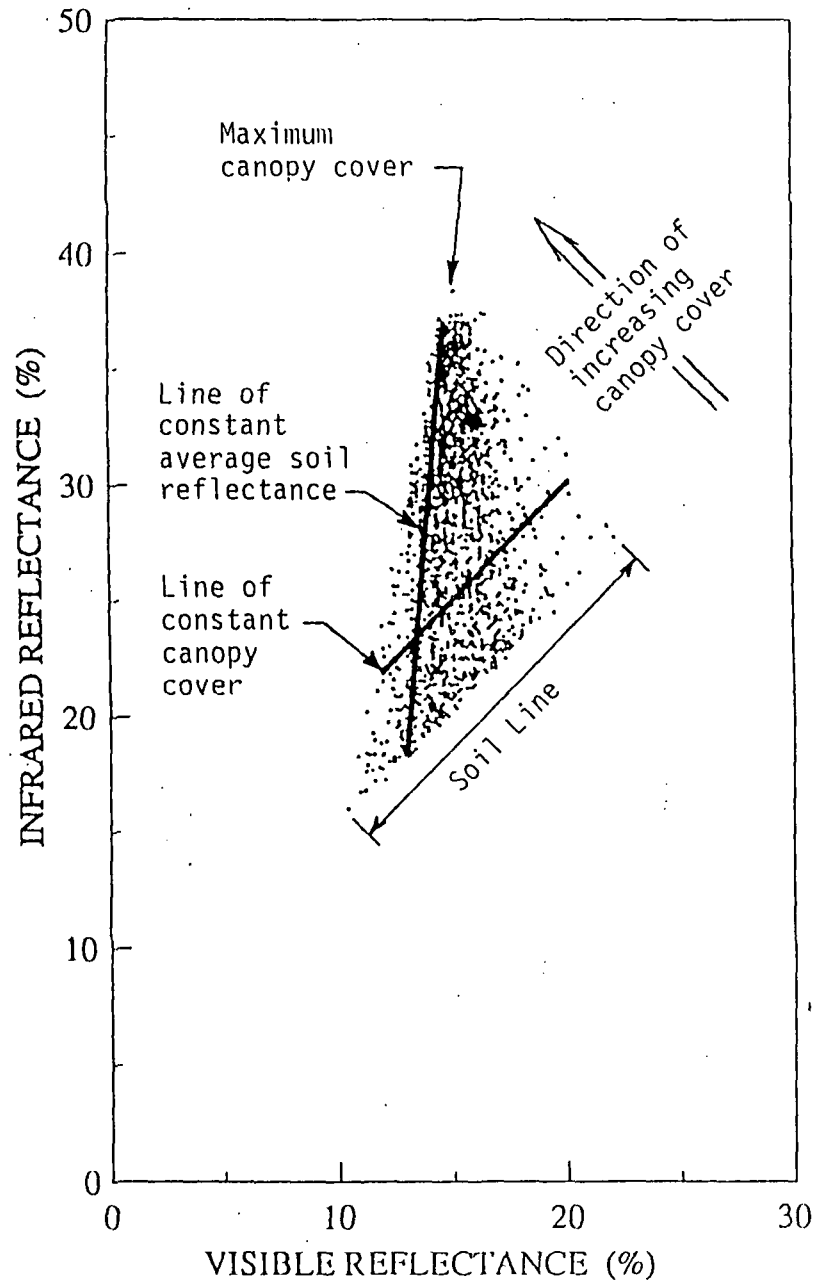
Hypotheses Testing. Most of the climatological, hydrological, and soils data required to test Eagleson's climate-soil-vegetation equilibrium hypotheses have been obtained for the Beaver Creek Basin in northern Arizona. Testing will begin shortly but its conclusion will require continued support.

Publications

Jasinski, M. F. and P. S. Eagleson, "The Structure of Visible-Infrared Scattergrams of Semivegetated Landscapes," submitted to IEEE Transactions on Geoscience and Remote Sensing. February, 1988.

Jasinski, M. F. and P. S. Eagleson, "Estimation of Subpixel Vegetation Cover Using Red-Infrared Scattergrams." In preparation.

Jasinski, M. F. and P. S. Eagleson, "The Physical Basis of Common Vegetation Indices for Semivegetated Landscapes." In preparation.



EXAMPLE CASE:

R_{VEG} 's constant

R_{SOIL} 's variable

Solar Zenith Angle = 30°

Tree Height = 5 m.

Tree Canopy Area = 1 sq. m.

Tree Location: Poisson Distribution
with variable rate

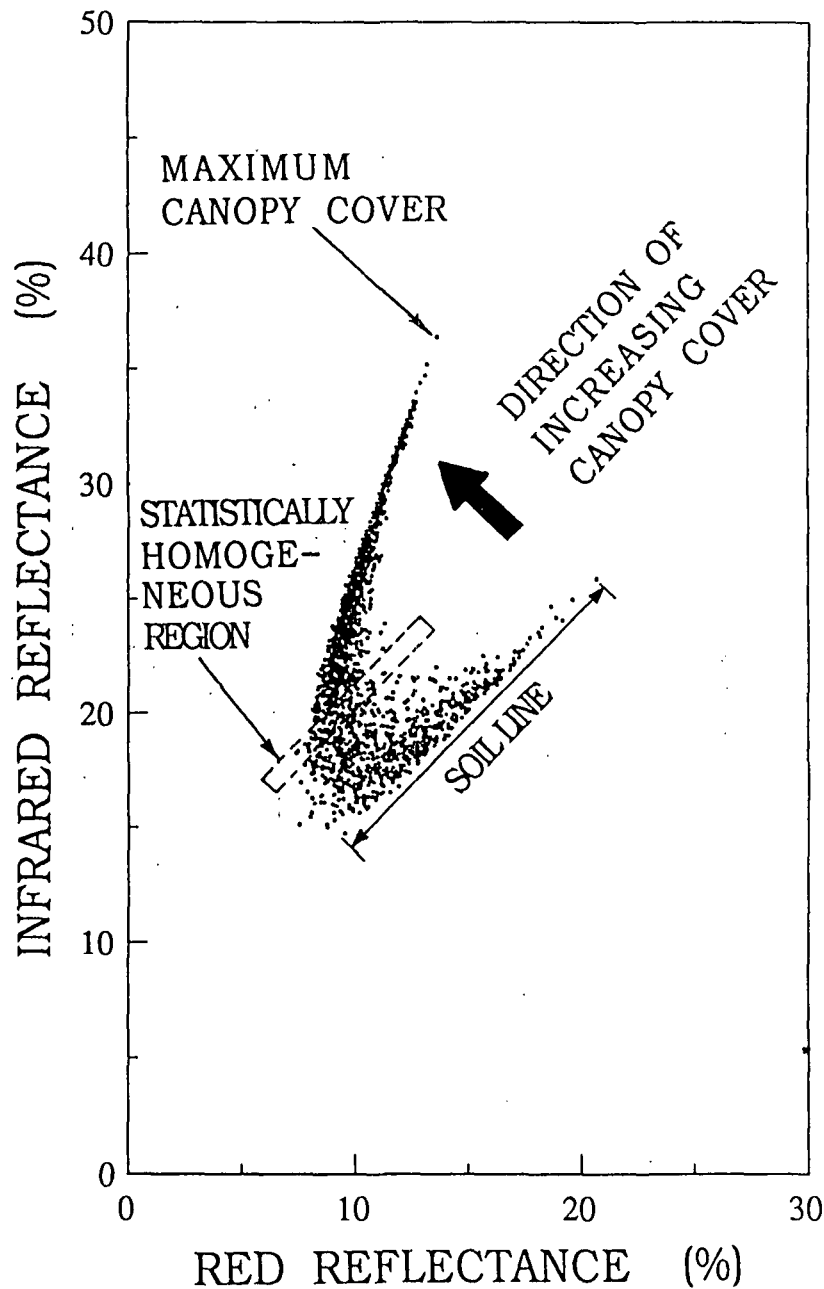
Pixel Area = $10 \times 10 = 100$ sq. m.

No Shadows

Figure 1

Red - Infrared Scattergram

Case II Simulation



EXAMPLE CASE:

R_{VEG} 's constant

R_{SOIL} 's variable

Solar Zenith Angle = 30°

Tree Height = 5 m.

Tree Canopy Area = 1 sq. m.

Tree Location: Poisson Distribution
with variable rate

Pixel Area = $10 \times 10 = 100$ sq. m.

Shadows

Figure 2

Red - Infrared Scattergram

Case V Simulation

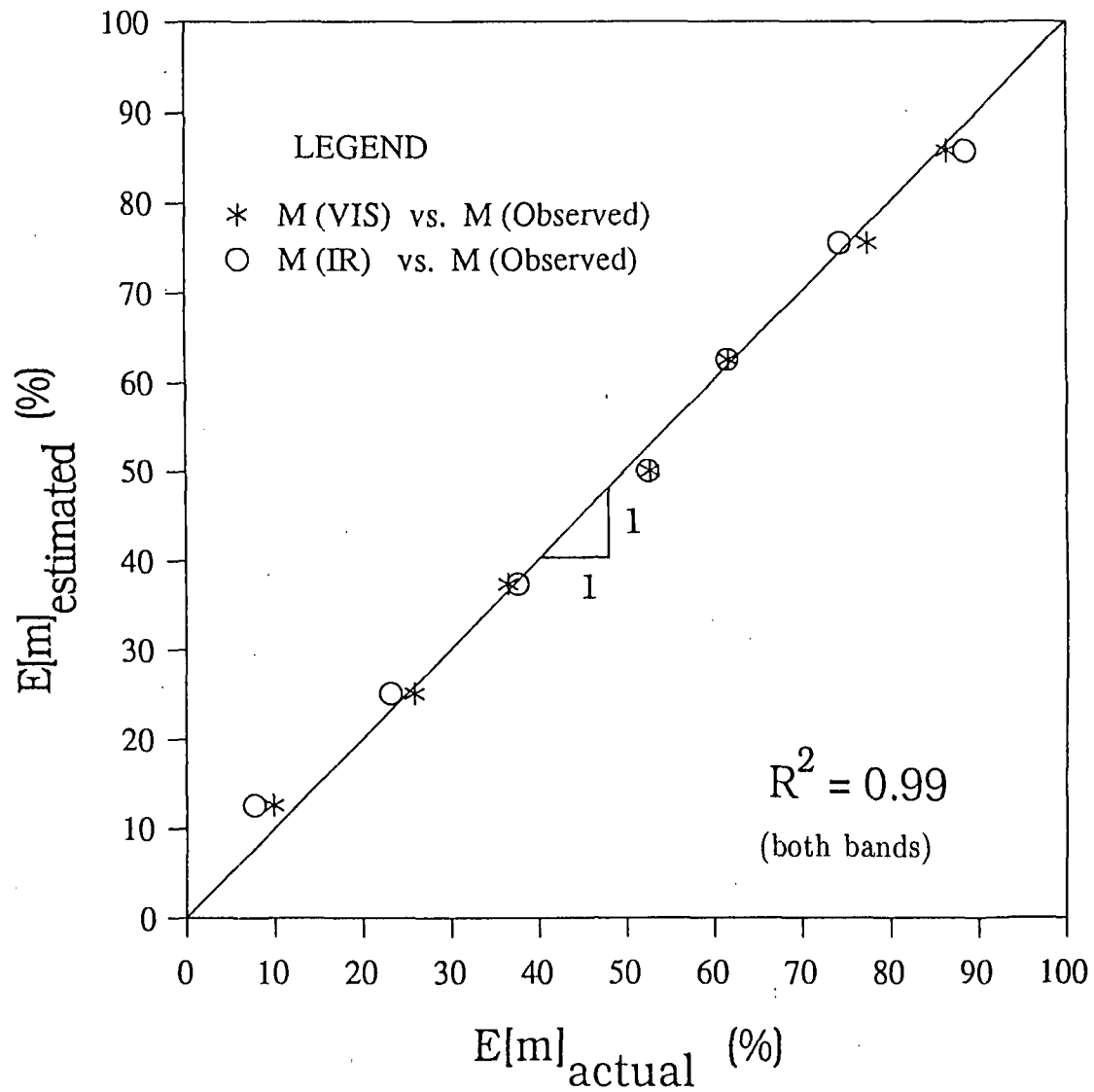


Figure 3. Estimated vs. Actual Mean Subpixel Canopy Cover
Case II Simulation

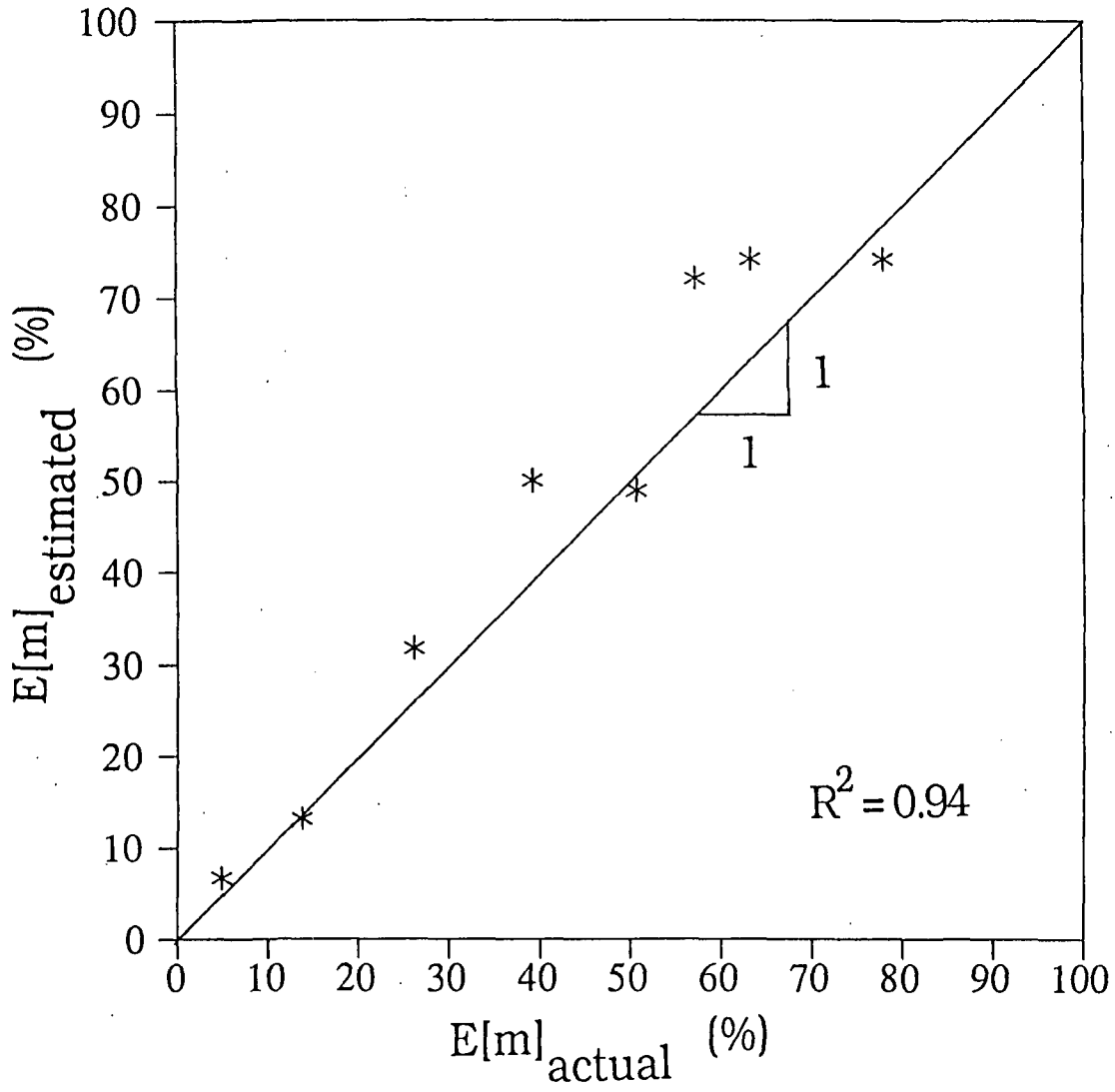


Figure 4. Estimated vs. Actual Mean Subpixel Canopy Cover
Case V Simulation

APPENDIX

THE STRUCTURE OF VISIBLE-INFRARED SCATTERGRAMS OF SEMIVEGETATED LANDSCAPES

Michael F. Jasinski and Peter S. Eagleson

ABSTRACT - A physically-based linear stochastic canopy-soil reflectance model is developed to investigate subpixel and regional variability of semivegetated landscapes. In particular, the model is used to investigate the structure of multidimensional scattergrams and to explain the often observed characteristic triangular shape of visible-infrared scattergrams of semivegetated landscapes. Scattergrams of simulated semivegetated scenes are analyzed with respect to the scales of the satellite pixel and subpixel components.

KEYWORDS - Canopy-soil reflectance model, remote sensing, semivegetated landscapes, stochastic processes, subpixel variability, scattergrams, soil line, tasseled cap.

Manuscript received _____; revised _____. This work was supported by NASA Goddard Space Flight Center under Grant NAG 5-510.

The authors are with the Ralph M. Parsons Laboratory for Water Resources and Hydrodynamics, Department of Civil Engineering, Massachusetts Institute of Technology, Cambridge, MA 02139.

Submitted to IEEE Trans. Geosci. and Remote Sens., February, 1988.

I. INTRODUCTION

The physically-based parameterization of heat and moisture fluxes from semivegetated landscapes is an unsolved problem in many mesoscale studies. One difficulty is quantifying state variables (e.g., vegetation cover, soil moisture, surface temperature) which exhibit important spatial and temporal variability at scales smaller than the scale of the measurement. Examples arise in the characterization, using satellite multispectral data, of semivegetated landscapes such as the semiarid regions of the southwest United States and agricultural lands during their early growing stages. In both cases vegetation density varies at characteristic scales (several meters) much smaller than the pixel scale of current satellite multispectral (MSS) sensors (several tens of meters). Pixel scale measurements represent the integrated reflectance of soil and vegetation, and as a result, techniques to disaggregate important subpixel components are warranted.

In addition to subpixel variations, many landscapes exhibit regional variations in soil and vegetation reflectance due to a variety of geoclimatic factors. For instance, changes in slope and aspect induce corresponding changes in scene reflectance through an effective altering in the illumination and viewing angles. Changes in elevation, slope, and aspect also cause scene variability through their indirect influence on such properties as soil moisture, and vegetation species and density. Thus, many soil and vegetation properties which exhibit small random subpixel scale fluctuations may be spatially correlated at larger geoclimatic scales. Knowledge of that correlation provides valuable insight into the solution of the parameterization problem.

This paper summarizes investigations of subpixel variability of regionally variable semivegetated landscapes using a linear stochastic canopy reflectance model. The purpose of the investigation is to develop a simple, physically-based, yet flexible means of characterizing both subpixel and regional variability without having to specify an inordinate number of plant and soil parameters, such as species, leaf angle and orientation, and soil roughness. Many of those parameters are of secondary importance to regional heat and moisture balance studies, and therefore can be absorbed into the statistical distribution of major variables such as plant size, percent vegetation cover, and vegetation and soil reflectance.

The present work demonstrates the utility of the canopy-soil reflectance model for interpreting the information content of multidimensional scattergrams through the use of simulated images. In particular, it examines the structure of the two-dimensional (visible-infrared) scattergram of semivegetated scenes, and the different mechanisms which contribute to its often observed characteristic triangular shape or "tasseled cap" [1]. Such understanding is invaluable to the solution of the inverse problem, the estimation of subpixel parameter variability given the observed scattergram.

II. REFLECTANCE OF INHOMOGENEOUS CANOPIES

The vegetation density of most landscapes varies both horizontally and vertically. The radiation reflected results from the complex scattering, absorption, and emittance properties of the plant components and soil background.

Physically-based radiative transfer models for horizontally homogeneous canopies have been developed in terms of leaf and soil hemispherical reflectances, leaf hemispherical transmittance, leaf area index, leaf inclination

angle distribution, and the fraction of diffuse incident solar radiation (for example, [2], [3], [4]). While such models provide a physical basis for understanding canopy reflectance, their application requires the estimation of a large number of parameters. For instance, Goel and Thompson [5] have demonstrated that the parameters of the Suits canopy reflectance model can be estimated using MSS data recorded for about 25 combinations of solar zenith angle and view angle. Thus, practical application of the technique using existing satellites is not possible due to the limited data currently available.

An alternative approach to modeling canopy reflectance with radiative transfer formulas is through the use of geometric models. These models, an evolution of early mixed pixel studies [6], conceptualize clumps of vegetation as solid three-dimensional geometric elements superposed on a flat soil background. The soil and vegetation are assumed to be lambertian surfaces and the total pixel reflectance depends upon the number, size, and spatial distribution of vegetation elements in the pixel.

Geometric models have been successfully used to describe much of the variability of actual and simulated scenes of vegetated landscapes. Otterman [7] focused on the relation between reflection from vertical plants and that from the planar surface. He modeled various vegetation types (forests, desert vegetation) as thin vertical cylinders of random height and spacing, introducing a geometric protrusion parameter as the fundamental unit characterizing canopy structure.

Richardson et al. [8] modeled crop canopies as rectangular rows, neglecting scattering between the crop and soil. They assumed that the total reflectance of an individual pixel was an area weighted sum of illuminated canopy reflectance, illuminated soil reflectance, and shadowed soil reflectance. Jackson et al. [9] extended the above model to include shadowed canopy effects.

Strahler and Li [10] and Li and Strahler [11] modeled conifer forests as randomly located cones of similar shape and random height. They demonstrated the feasibility of estimating several tree parameters of homogeneous areas using satellite data assuming constant tree and soil background reflectances.

Since geometric canopy models employ the whole plant as the fundamental unit of canopy structure (as opposed to leaves, stems, etc.), they are amenable to regional scale applications in which the spatial distribution of the plant can be prescribed. The statistical analysis of spatial patterns in botany has developed over the past fifty years (see for example, [12], [13]). Diggle [13] focused on the problem of fitting stochastic models to spatial point patterns of trees. He reviewed several investigations of the spatial patterns of trees and found that the most appropriate stochastic representation for a given situation was species dependent. For instance, the distribution of Japanese black pine saplings was found to follow a Poisson distribution. Redwood seedlings and bramble canes followed a Poisson cluster process.

Few researchers have incorporated the above information into the analysis of remotely sensed data. Significant progress in that direction has only recently been achieved [10], [11], [14]. Li and Strahler [11] and Strahler and Li [10] assumed a homogeneous Poisson distribution of conifer tree locations. Woodcock [14] used a similar model to examine the relation among the scale of pixel components, resolution size, and two indicators of spatial correlation: the variogram and the local variance.

III. SOIL REFLECTANCE

The spatial variability of soil reflectance is due to changes in complex scattering and absorption processes at the soil surface, as determined by its

physical structure and chemical composition. Major factors include mineral content, water and organic matter content, particle size, soil texture, surface roughness, and view angle. Numerous experimental investigations have examined the relationship between bare soil reflectance and those parameters (for a summary, see Myers [15]).

Soil reflectance variability manifests itself in multispectral scattergrams through the preferred location and orientation of bare soil pixels (see, for example, [1], [16], [17]). For visible-infrared scattergrams of typical semivegetated scenes, the data often take on the form of a triangle whose base consists of a straight line emanating from approximately the origin. Researchers have identified that base line, consisting primarily of pixels containing bare soil and dry vegetation, as the "soil line".

While the existence of the soil line has been attributed to the spatial variability of different soil properties, the important functional relationship between its shape and orientation, and the soil physical properties on which it depends, has received little attention. Such relationships can be established, however, using knowledge of soil reflectance behavior from previous theoretical and experimental studies (for example [18], [19], [20], [21]). That work indicates that for a given type of variability, the soil reflectance at one wavelength is often functionally related to the reflectance in another wavelength. In many cases, the relation can be approximated by a simple linear expression

$$R(\lambda_2) = \alpha R(\lambda_1) + \gamma \quad (1)$$

where the slope, α , and intercept, γ , are coefficients dependent on both the wavelength and the type of variability. Thus, variability of any one soil parameter can lead to a representative "line" in a two-dimensional scattergram.

For instance, Figure 1 contains three hypothetical visible-infrared scattergrams, representing three different scenes, in each of which only one soil parameter is allowed to vary. In Scene 1 only the amounts of two minerals are allowed to vary, while all other soil parameters such as surface roughness, moisture, etc. are held constant. The resulting scattergram forms a "soil mineral line" in which the end points approach the respective reflectances of the pure minerals. The shape and orientation of the line may be linear (as drawn) or nonlinear, and are determined by the location of the end points and the nature of the mixing of the two mineral types [22]. Pixels lying between the end points will contain mineral amounts proportional to their distance along the line.

Scene 2 contains hypothetical pixels in which only soil moisture is allowed to vary. Soil moisture increases the radiation capacity of the soil in the visible and near infrared regions. Analysis of published experimental data [20], [21], indicates that, for many soil types, equation (1) is applicable. Thus the locus of points for Scene 2 pixels should form a "soil moisture line" as indicated in Figure 1 with the pixels along the left portion of the line containing higher soil moisture than those to the right.

Finally, Scene 3 contains pixels in which only surface roughness varies. Soil reflectance generally decreases with increased surface roughness due to the increase in shadow cast by the soil particles and aggregates onto itself [15], [18]. The resulting "soil shadow line" is approximately linear with an intercept of near zero. The linearity occurs since the amount of shadow caused by the soil aggregates is practically the same for the range of wavelengths being considered. In fact, a near zero intercept for straight soil lines of real scenes (with low diffuse radiation) may be an indication that soil shadow induced by its physical structure is the dominant source of soil reflectance variability.

In actuality, real soil scenes contain a composite of several types of variability. The corresponding soil line is generally linear in the mean although considerable scatter can exist [1], [16]. A unique soil line will exist only if either 1) one dominant type of soil variability is occurring or 2) the scatter due to the different types of soil variability act in the same direction.

IV. STOCHASTIC CANOPY REFLECTANCE MODEL

This section presents a method for incorporating soil and vegetation variability which can occur over a range of length scales (subpixel to regional) into a geometric canopy-soil reflectance model. The model is used to simulate scenes which are then aggregated to various scales representative of typical satellite pixels. Once generated, scenes are analyzed in terms of the visible-infrared scattergrams. The main variables include vegetation and soil reflectance, percent vegetation cover, percent soil background, and percent shadow. An understanding of the role of each variable is obtained by its sequential introduction into the canopy cover model. Atmospheric effects are not considered. Five different cases are presented. The input parameters for each simulated scene are provided in Table 1.

The total reflectance of an individual pixel, R , is modeled as a linear combination of four main components; illuminated and shadowed canopy reflectance, and illuminated and shadowed soil background reflectance. It can be expressed in its most general form as

$$R[m_I, m_s, g_I, g_s, \bar{R}_{m_I}(\lambda), \bar{R}_{m_s}(\lambda), \bar{R}_{g_I}(\lambda), \bar{R}_{g_s}(\lambda)] =$$

$$m_I \bar{R}_{m_I}(\lambda) + m_s \bar{R}_{m_s}(\lambda) + g_I \bar{R}_{g_I}(\lambda) + g_s \bar{R}_{g_s}(\lambda) \quad (2)$$

where

λ = wavelength,

$\bar{R}_{m_I}(\lambda)$ = average reflectance of illuminated vegetation of a given pixel,

$\bar{R}_{m_S}(\lambda)$ = average reflectance of shadowed vegetation of a given pixel,

$\bar{R}_{g_I}(\lambda)$ = average reflectance of illuminated soil background of a given pixel,

$\bar{R}_{g_S}(\lambda)$ = average reflectance of soil background shadowed by canopy of a given pixel,

m_I, m_S = percentage of pixel covered with illuminated and shadowed canopy, respectively, and

g_I, g_S = percentage of pixel occupied by illuminated and shadowed soil background, respectively.

Average reflectances and percent covers are defined, for example

$$\bar{R}_{m_I}(\lambda) = \frac{1}{A} \int_A R_{m_I}(\lambda) dA_{m_I} \quad (3)$$

$$m_I = \frac{1}{A} \int_A dA_{m_I} \quad (4)$$

where

A = total area of a given pixel,

dA_{m_I} = area of smallest homogeneous element of illuminated canopy, and

$R_{m_I}(\lambda)$ = reflectance of smallest homogeneous element of illuminated canopy.

The total percent canopy cover, m , soil background, g , and shadow, s , in a pixel are, respectively,

$$m = m_I + m_S \quad (5)$$

$$g = g_I + g_S \quad (6)$$

$$s = m_S + g_S \quad (7)$$

where

$$m_I + m_S + g_I + g_S = 1 \quad (8)$$

Each scene consists of eight segments, each 150 meters square with one meter square pixels. Scenes are generated as follows. First, a soil background is assumed with a prescribed statistical distribution, including a covariance structure. Each segment of the scene contains the same soil background distribution. Next, trees represented by square cylinders of fixed height and diameter are superposed on the soil background of each segment according to a Poisson distribution having a different arrival rate for each segment. As for soil, a prescribed distribution for vegetation reflectance is assumed with a covariance structure. Typical values of soil and vegetation reflectivity are assumed [2], [15], [19] as indicated in Table 1. Finally, the original grid is aggregated to pixel sizes of 5, 10, and 30 meters square by averaging the reflectance values of the components of the grid. The latter two represent SPOT and Thematic Mapper satellite scales, respectively. Information regarding subpixel variables is recorded at each level of aggregation.

A. CASE I – CONSTANT REFLECTANCES, NO SHADOWS

This case represents an idealized two-component situation in which the vegetation and soil each have a constant reflectance over the entire scene, and observations are from the nadir. The sun is near zenith resulting in no shadows in the field of view. Hence, the only variable is percent cover. The equation

expressing total reflectance from an individual pixel is taken from equations (2) through (8) with $m_s = g_s = 0$, or

$$R[m, R_{m_I}(\lambda), R_{g_I}(\lambda)] = mR_{m_I}(\lambda) + (1 - m)R_{g_I}(\lambda) \quad (9)$$

The visible-infrared scattergrams for the Case I simulation are shown in Figures 2-a,b,c for the levels 5, 10, and 30 aggregation. They indicate that all the data points fall on a straight line whose end points represent pixels containing the maximum (upper left) and minimum (lower right) percent vegetation cover within the scene. The length of the line decreases with increasing aggregation since the standard deviation of the canopy density decreases as the pixel size increases. The percent cover of any pixel lying along the line is proportional to the distance between the end points. The end points do not necessarily represent pure vegetation or soil cover, but only the extreme coverages in the scene.

B. CASE II - VARIABLE SOIL REFLECTANCE, NO SHADOWS

In real scenes, variations in soil reflectance are apt to occur over a wide range of scales. For instance, spatial fluctuations in surface roughness are likely to occur at length scales of meters or centimeters. On the other hand, variations associated with slope, aspect, or basin geomorphology will occur at scales of tens of meters or greater.

In addition to changing vegetation cover, the Case II simulation includes the effect of spatial variability of soil reflectance. In order to simplify the analysis it is assumed that only one soil parameter is varying (i.e., surface roughness, mineral content, or soil moisture) and that there is no covariance between vegetation cover and soil reflectance.

In order to incorporate both small scale (subpixel) and large scale (regional) variations, soil reflectance in the Case II simulation is treated as a two-dimensional random field with a prescribed covariance structure. For instance, random fluctuations among adjacent elements in the simulated scene (level one aggregation) might correspond to small differences in surface roughness, while changes in slope, aspect, or basin geomorphology are characterized through the length scale of an appropriate covariance function:

While various functional forms might be applicable, for demonstration purposes the Case II simulation assumes that soil reflectance is normally distributed with an exponential covariance function. The exponential covariance function is expressed

$$\text{cov}(d) = \sigma^2 \exp(-\beta d) \quad (10)$$

where

σ^2 = the variance of the soil reflectance distribution,

β = inverse length scale of the covariance function, and

d = distance between two points in the scene.

The simulated bare soil scene for the visible band is shown in Figure 3. That scene, generated using the Turning Bands Method [23], contains a prescribed mean reflectance (0.15), standard deviation (0.023), and exponential covariance. A similar scene (not shown) was generated for the infrared band. The mean and standard deviations of both scenes are based on the hypothetical soil reflectance curve shown in Figure 4, which indicates a typical range of reflectances for a soil with variable properties (e.g., soil moisture or surface roughness) [15], [20].

The length scale of the exponential covariance function was chosen to be 20 meters. While that might represent some geophysical scale, for the present case it

is chosen for convenience. It is much larger than the grid scale of one meter, and the two smaller aggregations (5 and 10 meters), but smaller than the largest aggregation (30 meters). Thus, the choice of that scale allows one to examine the relation between covariance length scale and pixel size.

The total reflectance from a given pixel in the Case II simulation is,

$$R[m, R_{m_I}(\lambda), \bar{R}_{g_I}(\lambda)] = mR_{m_I}(\lambda) + (1 - m)\bar{R}_{g_I}(\lambda) \quad (11)$$

The results of the Case II simulation for all three aggregations are shown in Figures 5-a,b,c. (Regular spaces in the scattergrams, especially at lower level aggregations, are due to finite increments in percent cover as limited by the level of aggregation. This effect occurs in subsequent cases as well.) They indicate that the visible-infrared scattergram tends to take on the characteristic shape of a triangle. The top of the triangle represents full canopy cover, and the base represents the minimum vegetation cover in the scene. For areas in which it can be assumed that bare soil exists, the base of the triangle represents the classic "soil line."

While Case II is still a relatively simple example, it demonstrates the usefulness of the scattergram for explaining subpixel variability. For instance, the percent cover of any pixel lying within the triangle is approximately proportional to its distance between the top of the triangle and the soil line. An equivalent statement is that all pixels falling on a line parallel to the soil line will have the same percent vegetation. A second observation is that all pixels falling on a straight line emanating from the top of the triangle will have the same value of average soil reflectance. The above interpretations of the scattergram are indicated on Figure 6 (an expanded version of 5b) for the level 10 aggregation.

The importance of pixel scale relative to the covariance function is seen in the size of the triangles at different levels of aggregation. The scattergrams indicate that the length of the soil line and hence the width of the triangle decrease with increasing aggregation. Both the standard deviation and the covariance length scale contribute to that effect. Since scenes composed of large pixels average over a greater area than scenes with small pixels, statistically, one can expect the former case to have a lower standard deviation. However, that effect is mitigated by the covariance length scale. Scenes with small length scales (relative to pixel size) will exhibit short soil lines while scenes with large length scales will exhibit long soil lines.

C. CASE III – VARIABLE VEGETATION REFLECTANCE, NO SHADOWS

In addition to variable percent cover and variable soil reflectance, the Case III simulation introduces variable vegetation reflectance and examines its effect on the visible-infrared scattergram. Vegetation reflectance will change at small and large spatial scales due to variations in a number of plant parameters, including plant species, leaf reflectance, growth stage, plant architecture, leaf orientation and distribution, leaf area, and plant stress [2]. Regional scale variations in the pattern of natural vegetation and dominant species are influenced by elevation, gradient, and local climate [12].

As for soil, Case III treats the variation in vegetation reflectance as a normally distributed random variable with an exponential covariance structure. It further assumes that reflectances in the infrared and visible bands are linearly related with negative slope. That relationship is not intended to represent all types of vegetation variability, but may be a simple approximation for some cases. For instance, increases in leaf area are generally associated with decreases in visible reflectance and increases in infrared reflectance (see for example, [24]. [25]).

For Case III, the total reflectance of a given pixel becomes

$$R[m, \bar{R}_{m_I}(\lambda), \bar{R}_{g_I}(\lambda)] = m\bar{R}_{m_I}(\lambda) + (1 - m)\bar{R}_{g_I}(\lambda) \quad (12)$$

where the three random variables are percent cover (m), vegetation reflectance (\bar{R}_{m_I}) and soil reflectance (\bar{R}_{g_I}).

The scattergram for Case III is presented in Figures 7-a,b,c for all levels of aggregation. The difference from Case II is that the top of the triangle has spread open, resulting in a quadrilateral data plot. An envelope curve along the top of the quadrilateral represents pixels of maximum vegetation cover. For scenes containing full canopy cover, that locus of points can be considered the "canopy line" analogous to the soil line at the base of the quadrilateral.

D. CASE IV - SHADOWED SOIL BACKGROUND, CONSTANT VEGETATION AND SOIL REFLECTANCE

Shadows cast by vegetation are an important component of total pixel reflectance. Shadows change diurnally with the position of the sun and with the amount of atmospheric scatterers which affect diffuse solar radiation. Important seasonal changes occur both with the sun's migration and with changes of plant structure.

Case IV examines the effect of shadows cast by plants on soil. That is achieved by conceptualizing plants as vertical square cylinders, with horizontal tops and equal height of five meters. Solar and view angles are assumed to be 30° and 0°, respectively.

The reflectance equation for a given pixel is

$$\begin{aligned} R[m, g_I, g_S, R_{m_I}(\lambda), R_{g_I}(\lambda), R_{g_S}(\lambda)] &= \\ &= mR_{m_I}(\lambda) + g_I R_{g_I}(\lambda) + g_S R_{g_S}(\lambda) \end{aligned} \quad (13)$$

The scattergrams associated with the three aggregation levels for the Case IV simulation are shown in Figures 8-a,b,c. They reveal several interesting relations among percent cover and shadow, the level of aggregation, and the characteristic shape of the scattergram.

All the data pairs fall within a space defined by a triangle. This is illustrated using the level 5 aggregation as indicated in Figure 9 (an expanded version of 8a). The vertices of the triangle (labeled Points B, C, and D) correspond to the assumed pure spectra of the full shadow (reflectance = 0.0), full canopy, and pure soil, respectively, as indicated in Table 1.

Since pixels located within the triangle are linear mixtures of the three cover types, the exact percentage of any cover type can be determined on the basis of its location in the scattergram.

For instance, the percent covers for an arbitrary pixel A shown on Figure 9 can be determined graphically as follows. First, lines EF and GH are drawn through pixel A parallel to CD and BD, respectively. It is then noted that line EF is located about one-third of the distance between the line CD and point B. That indicates that pixel A contains 33 percent shadow. Line GH is situated about one-fourth the distance between the line BD and point C, indicating that pixel A has 25 percent vegetation cover. The remaining cover, 42 percent, is bare soil, which can be checked on the basis of pixel A's location between line BC and point D.

The above determination of the three cover types is simply a graphical illustration of an analytical solution applicable within the limits of the Case IV assumptions. It can be applied to any level of aggregation. The solution could also be achieved algebraically using equation (13) for both wavelengths (two equations) and equation (8).

The Case IV scattergrams also reveal an important relation between shadow length scale and pixel size. For instance, at the level 5 aggregation, since the length scale of the shadow is about the same or greater than the pixel scale, there are numerous instances when the shadow of a tree in one pixel falls onto an adjacent pixel. The three components of the pixel (vegetation, shadowed soil and illuminated soil) are then independent of each other in a majority of cases. As a result, pixels can occupy almost any space within the limits of the triangular scattergram given a large enough sample size.

However, as the level of aggregation increases, the length scale of the shadows becomes much smaller than the size of the pixel. As a result, shadows associated with a given tree fall increasingly within the same pixel and the amount of ground shadow becomes uniquely related to the amount of vegetation cover. Mathematically, that dependence among the three cover variables is expressed

$$g_s = g_s(m) \quad (14)$$

$$g_I = g_I(m) = 1 - m - g_s(m) \quad (15)$$

and equation (15) becomes

$$R(\lambda, m, g_I, g_s) = R[\lambda, m, g_I(m), g_s(m)] \quad (16)$$

A major consequence of the above relations is that it reduces the feasible region in the scattergram. Even at the level 5 aggregation (Figure 8a), that effect is manifested as a slight indentation in the upper right hand side of the triangular

scattergram. At higher levels of aggregation, Equation (16) implies that there is only one position in the scattergram associated with a given canopy cover. As a result, one should expect the triangular scattergram observed at the level 5 aggregation to collapse to a single curved line when the shadow length scale becomes small relative to the pixel size. That is indeed shown to be true in a progressive manner by examining the sequential shapes of the scattergrams in Figure 8b (level 10 aggregation) and Figure 8c (level 30 aggregation).

Since shadow length scale is inherently a function of canopy height and geometry, solar angle, and ground slope, understanding its effect on visible-infrared scattergrams is vital to the interpretation of multispectral scenes.

E. CASE V – SHADOWED SOIL BACKGROUND, VARIABLE SOIL REFLECTANCE

Case V is a more realistic version of the shadow model in which soil reflectance is assumed normally distributed as in Case II. The governing equation for an individual pixel is

$$\begin{aligned}
 R[m, g_I, g_S, R_{m_I}(\lambda), \bar{R}_{g_I}(\lambda), R_{g_S}(\lambda)] &= \\
 &= mR_{m_I}(\lambda) + g_I\bar{R}_{g_I}(\lambda) + g_S R_{g_S}(\lambda)
 \end{aligned}
 \tag{17}$$

The resulting scattergrams for the different levels of aggregation are shown in Figure 10.

The scattergrams of the Case V simulation represent a combination of the effects illustrated in Case II (constant vegetation reflectance, variable soil reflectance) and Case IV (shadow effects).

For instance, the scattergram of the level 5 aggregation, Figure 10a, exhibits a triangular shape overall, but with a pronounced indentation in the upper right portion due to the shadow effects. It can be regarded as a superposition of many triangular scattergrams, each for a homogeneous soil (constant background reflectance), similar to that of Case IV, level 5 aggregation (Figure 9). That is illustrated in Figure 11 (expanded version of 10a). Those triangles share two common vertices at 1) the point of pure shadow reflectance (point B), and 2) the point of pure vegetation reflectance (point C). The third vertex (labeled D_1 , D_2 , D_3 , ... etc.) is unique for each triangle, representing the reflectivity of a particular soil which is homogeneous at that aggregation. The collection of all vertices, D , constitutes the true soil line.

In the particular example shown, the true soil line has an intercept greater than zero, and is thus situated slightly inside the boundaries of the overall scattergram, as indicated in Figure 11. It is also possible, however, that the shadowed soil reflectance lies above the soil line. Only in such cases will the bottom of the scattergram accurately represent the true soil line.

An important consequence of the level 5 aggregation is that pixels containing different mixtures of vegetation, shadow, and variable soil can occupy the same location in the scattergram. As a result, the percent cover of individual pixels can not be determined explicitly as shown in previous examples.

The scattergrams of the levels 10 and 30 aggregation are shown in Figures 10b and 10c, respectively. As in Case IV, because of the unique relation between shadow and vegetation cover at this scale, the scattergrams collapse progressively to the shape of a "tasseled cap" [1]. At the level 30 aggregation, the scattergram consists of a series of juxtaposed curved lines, each line possessing constant average soil reflectivity (similar to Case IV, level 30 aggregation, Figure 8c), extending

from individual points on the true soil line to the tip of the tasseled cap. That is illustrated in Figure 12 (expanded version of 10c).

Unlike the level 5 aggregation, percent cover can be estimated for Case V, level 30 aggregation, in a manner similar to Cases II and IV. Percent cover is proportional to the distance between the soil line and the tip of the tasseled cap.

VI. SUMMARY

In many semivegetated regions, important spatial fluctuations in vegetation and soil reflectance can occur at scales much smaller than the pixel scale of current satellite multispectral sensors. At the same time, regional variations can occur due to geoclimatic factors. This report has demonstrated a flexible, physically-based approach for characterizing both subpixel and regional spatial variability through the development of a stochastic geometric canopy reflectance model.

A principal feature of the model is the inclusion of randomness and spatial correlation in both the percent cover and reflectance terms. It is argued that many plant and soil parameters which contribute to scene reflectance variability can be absorbed into a few major variables. As a result, the model is amenable to the investigation of the spatial variability of real scenes which are too complex to study in a completely deterministic manner.

Although several applications of the canopy reflectance model are envisioned, this report has focused on understanding the physical basis of the shape of multidimensional scattergrams. In particular, the role that percent vegetation cover, shadows (cast by vegetation on soil), and soil and vegetation reflectance play in the evolution of the typical triangular shape of visible-infrared scattergrams of vegetated scenes has been demonstrated.

Several characteristics of semivegetated landsurfaces lead to triangular scattergrams, although perhaps the most important condition is the existence of vegetation of constant reflectivity and variable amount, without shadows, on a soil background of variable reflectance (Case II). The triangular shape is observed at all levels of aggregation, although the length of the soil line decreases with increasing aggregation, in accordance with its covariance structure. Percent vegetation cover of a given pixel is proportional to its distance from the soil line.

For scenes characterized by shadows and constant reflectivities (Case IV), a different triangular scattergram than above can occur when the length scale of the shadow is about the same as or greater than the pixel size. Under those circumstances, shadows cast by vegetation of a given pixel are apt to fall on adjacent pixels. However, scattergrams formed in this manner should collapse to a single curved line at higher aggregations.

For scenes characterized by constant vegetation reflectance, variable cover, shadows, and variable soil background reflectance (Case V), a triangular scattergram exists at all levels of aggregation. However, it collapses progressively to a classic "tasseled cap" as the pixel scale becomes greater than the shadow length.

Although only relatively simple scenes have been investigated, they illustrate the utility of the model for examining important elements of the scattergram. The model can easily be extended to include other factors, including, for example, variations in leaf area, plant geometry, and the effect of shadows cast on vegetation. The effect of alternative spatial distributions can also be easily investigated.

A potential application of the model is the solution to the inverse problem, the estimation of subpixel variability of real satellite derived scenes.

Two features make that possible. First, the joint analysis of multispectral bands, as illustrated with the scattergrams, provides additional physically-based equations without necessarily adding new unknowns. Second, the analysis requires only one (cloud-free) scene, thereby avoiding the cumbersome task of registering several multiview scenes required by some inversion techniques. This research application is currently under way and will be summarized in a subsequent report.

REFERENCES

- [1] R. J. Kauth and G. S. Thomas, "The Tasselled Cap—A Graphic Description of the Spectral–Temporal Development of Agricultural Crops as Seen by Landsat," *Proc. of the Symp. on Machine Processing of Remotely Sensed Data*, Purdue Univ., W. Lafayette, IN, pp. 4B41–4B51, 1976.
- [2] J. Ross, *The Radiation Regime and Architecture of Plant Stands*, Dr. W. Junk, Publishers, The Hague, 1981.
- [3] G. H. Suits, "Calculation of the Directional Reflectance of a Vegetation Canopy," *Remote Sensing of Environment*, Vol. 2, pp. 117–125, 1972.
- [4] W. Verhoef, and N. J. J. Bunnik, "Influence of Crop Geometry on Multispectral Reflectance Determined by Use of Canopy Reflectance Models," *Proceedings of the International Colloquium on Signatures of Remotely Sensed Objects*, Avignon, pp. 273–290, 1981.
- [5] N. S. Goel and R. L. Thompson, "Inversion of Vegetation Canopy Reflectance Models for Estimating Agronomic Variables. III. Estimation Using Only Canopy Reflectance Data as Illustrated by the Suits Model," *Remote Sensing of Environment*, Vol. 15, pp. 223–236, 1984.
- [6] H. M. Horwitz, R. F. Nalepka, P. D. Hyde, and J. P. Morgenstern, "Estimating the Proportions of Objects within a Single Resolution Element of a Multispectral Scanner," *Proceedings of the 6th International Symposium on Remote Sensing of Environment*, Willow Run Labs, The University of Michigan, Ann Arbor, MI, pp. 1307–1320, 1971.
- [7] J. Otterman, "Albedo of a Forest Modeled as a Plane with Dense Protrusions," *Journal of Climate and Applied Meteorology*, Vol. 23, February, pp. 297–307, 1984.

- [8] A. J. Richardson, C. L. Wiegand, H. W. Gausman, J. A. Cuellar, and A. H. Gerbermann, "Plant, Soil, and Shadow Reflectance Components of Row Crops," *Photogrammetric Engineering and Remote Sensing*, Vol. 41, No. 11, pp. 1401–1407, 1975.
- [9] R. D. Jackson, R. J. Reginato, P. J. Pinter, and S. B. Idso, "Plant canopy information extraction from composite scene reflectance of row crops," *Applied Optics*, Vol. 18, No. 22, pp. 3775–3782, 1979.
- [10] A. H. Strahler and Li Xiaowen, "An Invertible Coniferous Forest Canopy Reflectance Model," *Proceedings of Fifteenth International Symposium on Remote Sensing of Environment*, Ann Arbor, MI, pp. 1237–1244, 1981.
- [11] X. Li and A. H. Strahler, "Geometric–Optical Modeling of a Conifer Forest Canopy," *IEEE Transactions on Geoscience and Remote Sensing*, Vol. GE–23, No. 5, pp. 705–721, 1985.
- [12] R. H. Whittaker, *Communities and Ecosystems*, 2nd Edition, Macmillan Publishing Co., New York, 1975.
- [13] P. J. Diggle, *Statistical Analysis of Spatial Point Patterns*, Academic Press, New York, 1983.
- [14] C. E. Woodcock, *Understanding Spatial Variation in Remotely Sensed Imagery*, Ph.D. Dissertation, University of California, Santa Barbara, 1985.
- [15] V. I. Myers, "Remote Sensing Applications in Agriculture," in *Manual of Remote Sensing*, American Society of Photogrammetry, Chapter 33, pp. 2111–2228, 1983.
- [16] A. J. Richardson and C. L. Wiegand, "Distinguishing Vegetation from Soil Background Information," *Photogrammetric Engineering and Remote Sensing*, Vol. 43, No. 12, pp. 1541–1552, 1977.

- [17] A. R. Huete, R. D. Jackson and D. F. Post, "Spectral Response of a Plant Canopy with Different Soil Backgrounds," *Remote Sensing of Environment*, Vol. 17, pp. 37-53, 1985.
- [18] J. Cierniewski, "A Model for Soil Surface Roughness Influence on the Spectral Response of Bare Soils in the Visible and Near-Infrared Range," *Remote Sensing of Environment*, Vol. 23, pp. 97-115, 1987.
- [19] J. A. Smith, "Matter-Energy Interaction in the Optical Region," in *Manual of Remote Sensing*, American Society of Photogrammetry, Chapter 3, pp. 61-113.
- [20] S. A. Bowers and R. J. Hanks, "Reflection of Radiant Energy from Soils," *Soil Science*, Vol. 100, No. 2, pp. 130-138, 1965.
- [21] E. L. Skidmore, J. D. Dickerson and H. Schimmelpfennig, "Evaluating Surface-Soil Water Content by Measuring Reflectance," *Soil Sci. Soc. Amer. Proc.*, Vol. 39, pp. 238-242, 1975.
- [22] M. D. Smith, P. E. Johnson, and J. B. Adams, "Quantitative Determination of Mineral Types and Abundances from Reflectance from Reflectance Spectra Using Principal Components Analysis," *Proc. 15th Lunar and Planetary Science Conference, Part 2, J. of Geoph. Res.*, Vol. 20, Supplement, pp. C797-C804, 1985.
- [23] A. Mantoglou and J. L. Wilson, "The Turning Bands Method for Simulation of Random Fields Using Line Generation by a Spectral Method," *Water Resources Research*, Vol. 18, No. 5, pp. 1379-1394, 1982.
- [24] J. E. Colwell, "Vegetation Canopy Reflectance," *Remote Sensing of Environment*, Vol. 3, pp. 175-183, 1974.
- [25] F. Hall, "Remote Sensing of Vegetation at Regional Scales," *Proc. Soc. Photo-Optical Instrum. Eng.*, Vol. 475, pp. 81-96, 1984.

Table 1
Summary
Input Parameters of Simulated Scenes

<u>Case</u>	Vegetation Reflectance Parameters <u>1/</u>					Soil Reflectance Parameters						
	Visible		Infrared		Covariance	Visible		Infrared		Spatial	Covariance	Shadow
	<u>Mean</u>	<u>S.Dev.</u>	<u>Mean</u>	<u>S.Dev.</u>	<u>Structure</u>	<u>Mean</u>	<u>S.Dev.</u>	<u>Mean</u>	<u>S.Dev.</u>	<u>Distribn.</u>	<u>Structure</u>	
I	0.15	0.00	0.40	0.00	none	0.20	0.00	0.25	0.00	uniform	none	No
II	0.15	0.00	0.40	0.00	none	0.15	0.023	0.20	0.023	normal	exponential b = 20 m	No
III	0.15	0.02	0.40	0.04	exponential b = 10 m	0.15	0.023	0.20	0.023	normal	exponential b = 20 m	No
IV	0.15	0.00	0.40	0.00	none	0.20	0.00	0.25	0.000	uniform	none	Yes <u>2/</u>
V	0.15	0.00	0.40	0.00	none	0.15	0.023	0.20	0.023	normal	exponential b = 20 m	Yes <u>2/</u>

1/Trees distributed according to a Poisson process with variable rate; tree height assumed to be 5 meters.

2/Solar angle assumed to be 30 degrees.

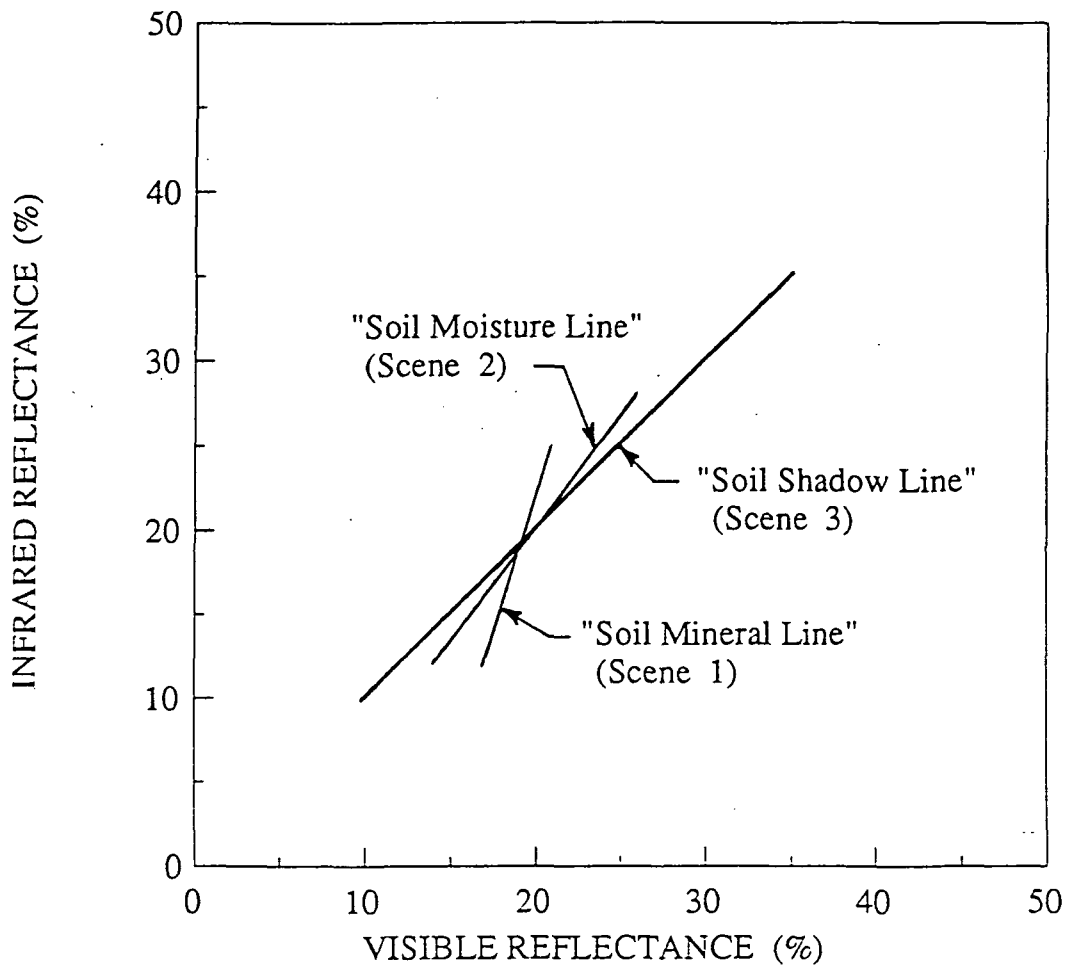


Figure 1. Hypothetical soil lines.

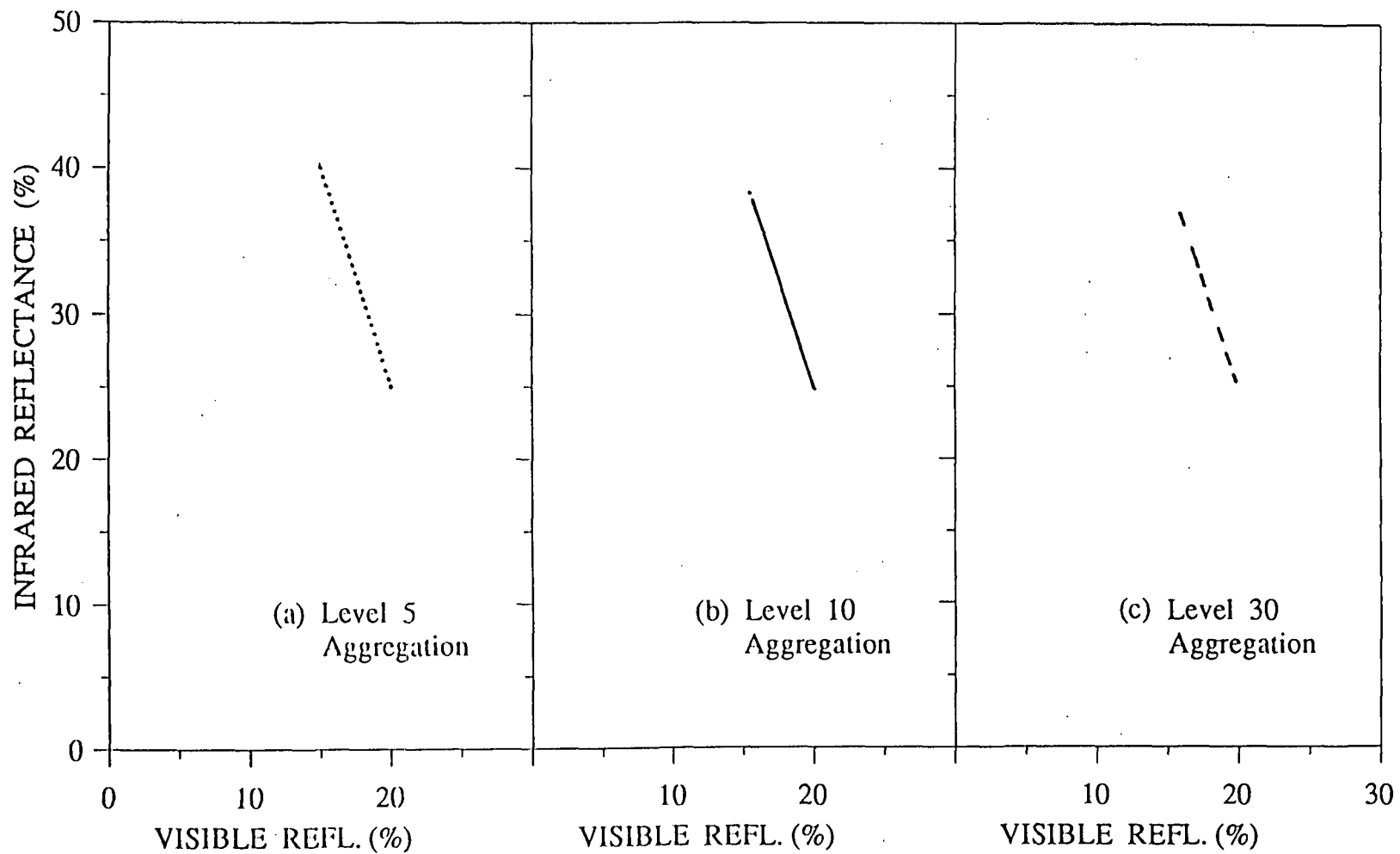


Figure 2--a,b,c. Visible-infrared scattergrams, Case I simulation: variable percent cover, constant soil and vegetation reflectances; no shadows.

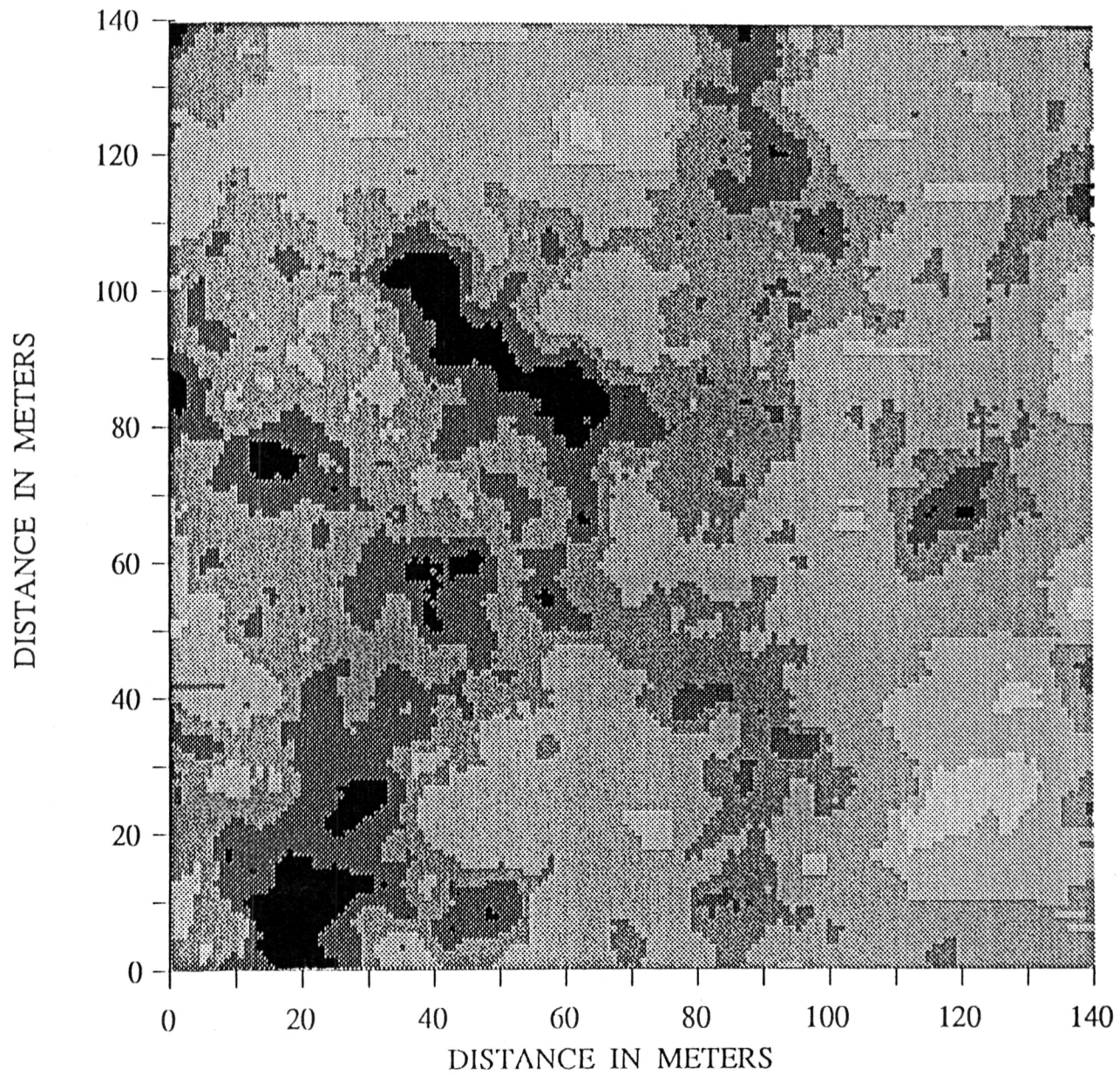


Figure 3. Hypothetical segment of bare soil scene, visible band.

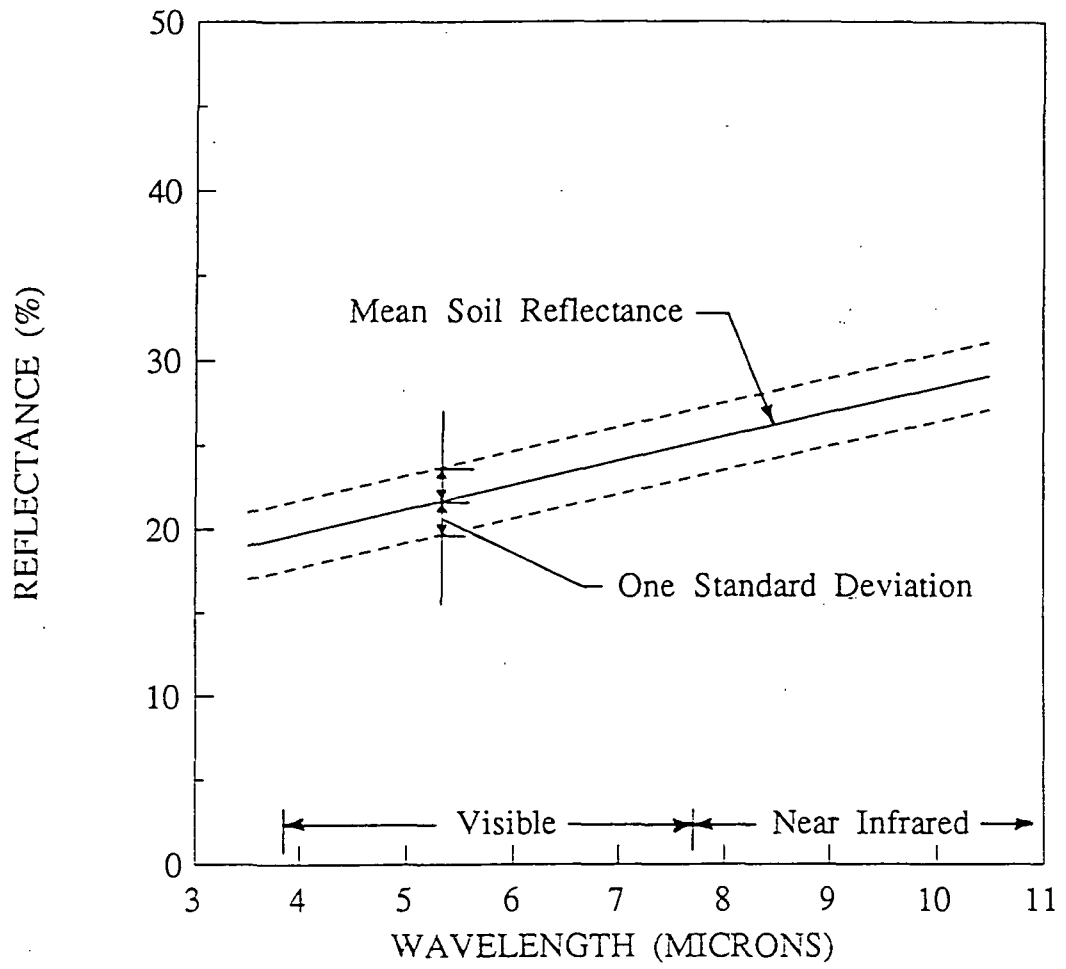


Figure 4. Hypothetical soil reflectance curve.

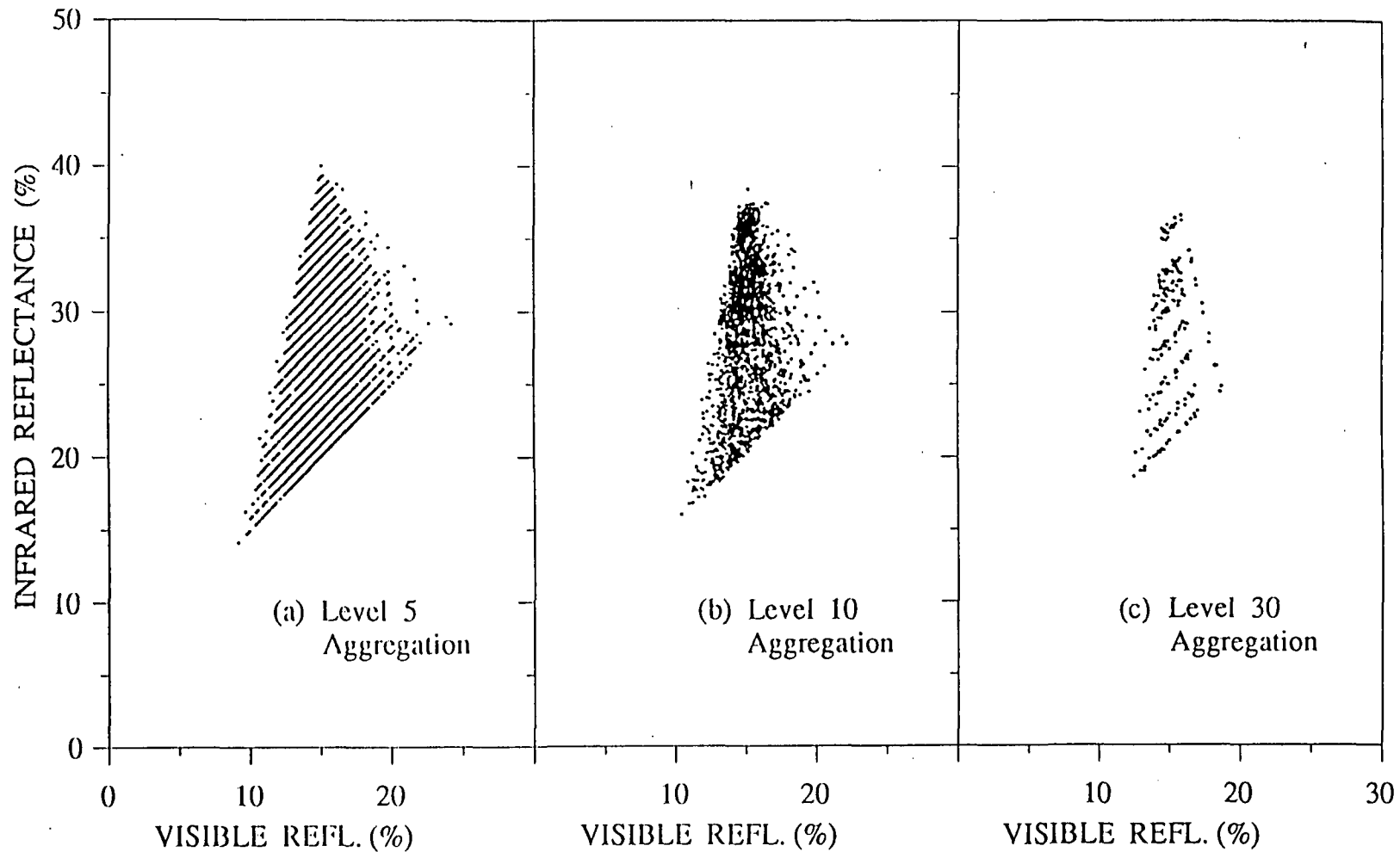


Figure 5-a,b,c. Visible-infrared scattergrams, Case II simulation: variable percent cover and soil reflectance, constant vegetation reflectance; no shadows.

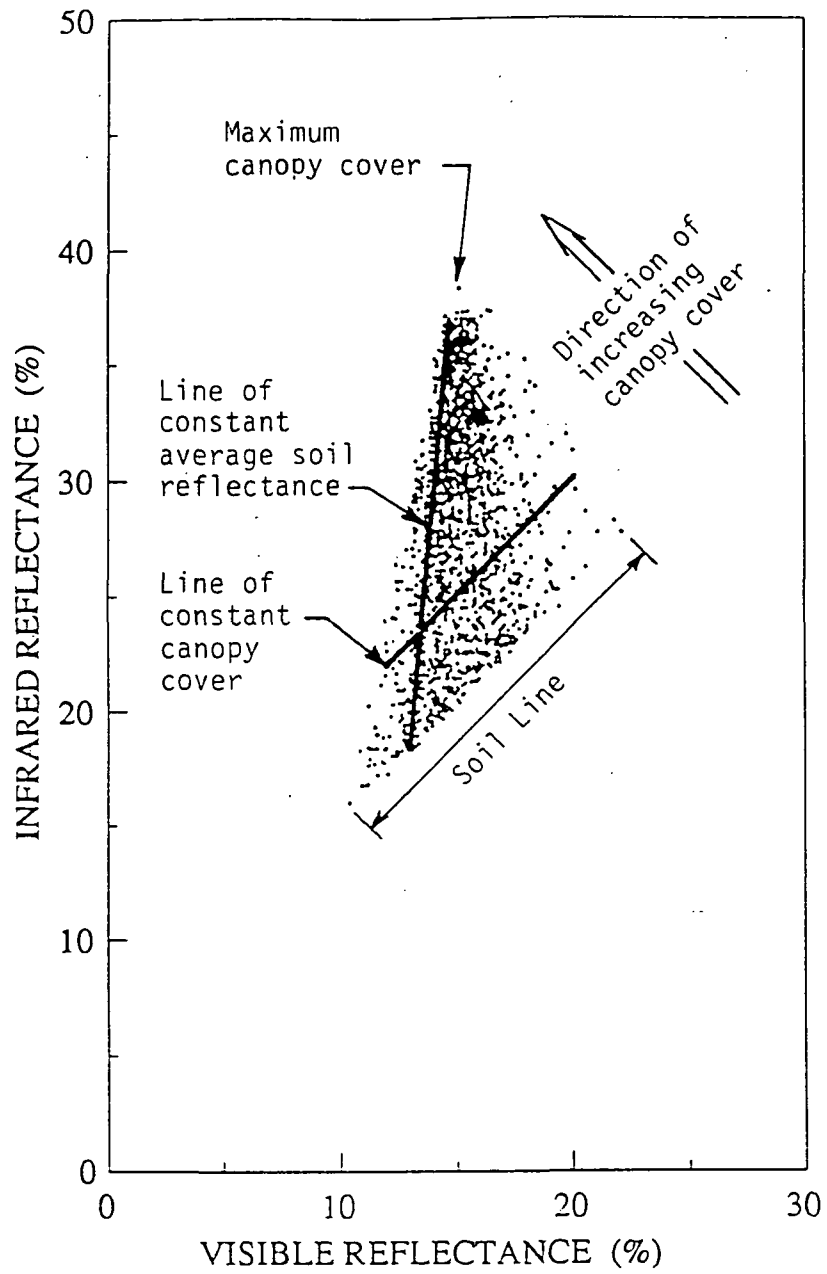


Figure 6. Interpretation of scattergram, Case II simulation, level 10 aggregation: variable percent cover and soil reflectance, constant vegetation reflectance; no shadows.

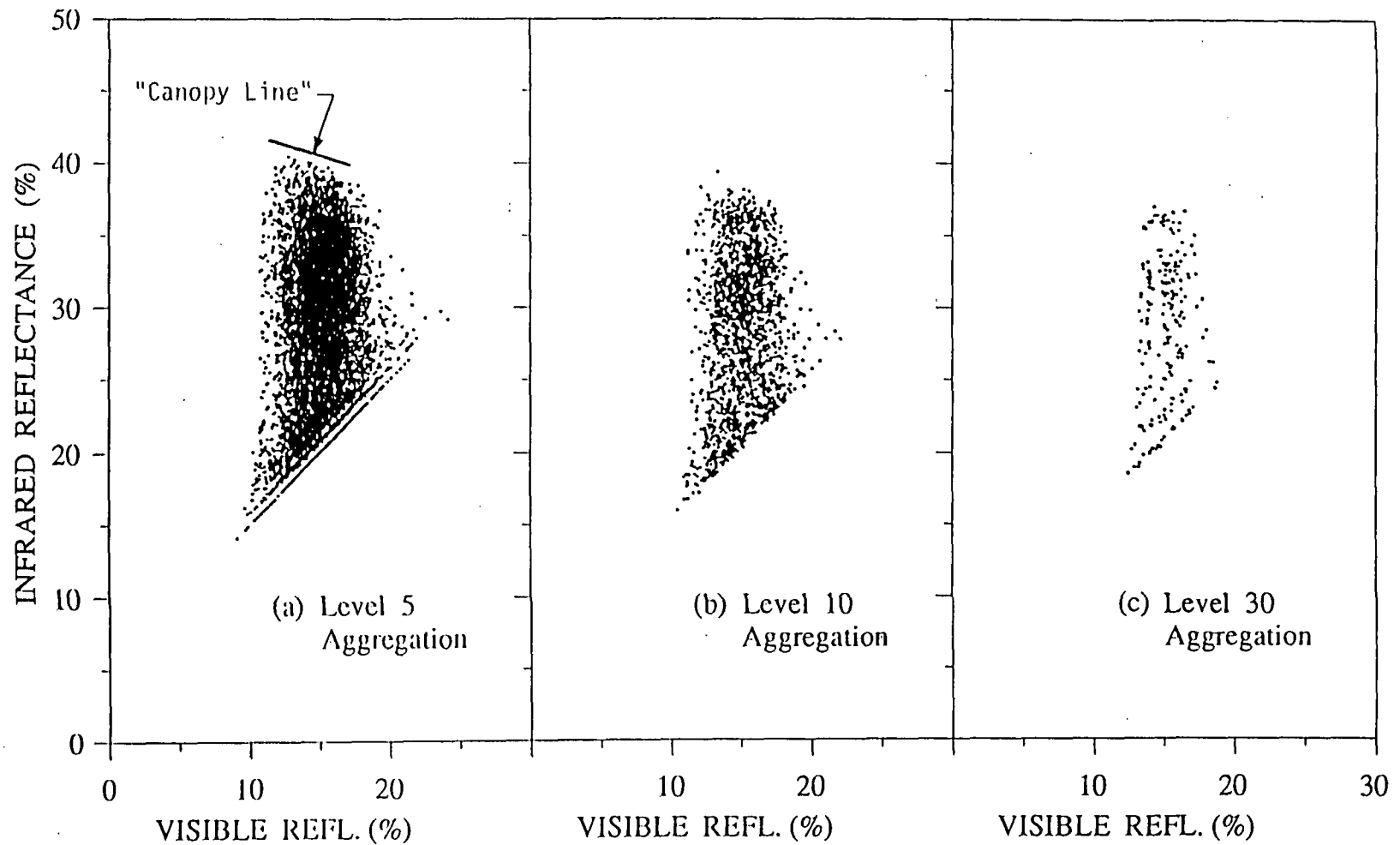


Figure 7-a,b,c. Visible-infrared scattergrams, Case III simulation: variable percent cover, soil and vegetation reflectances; no shadows.

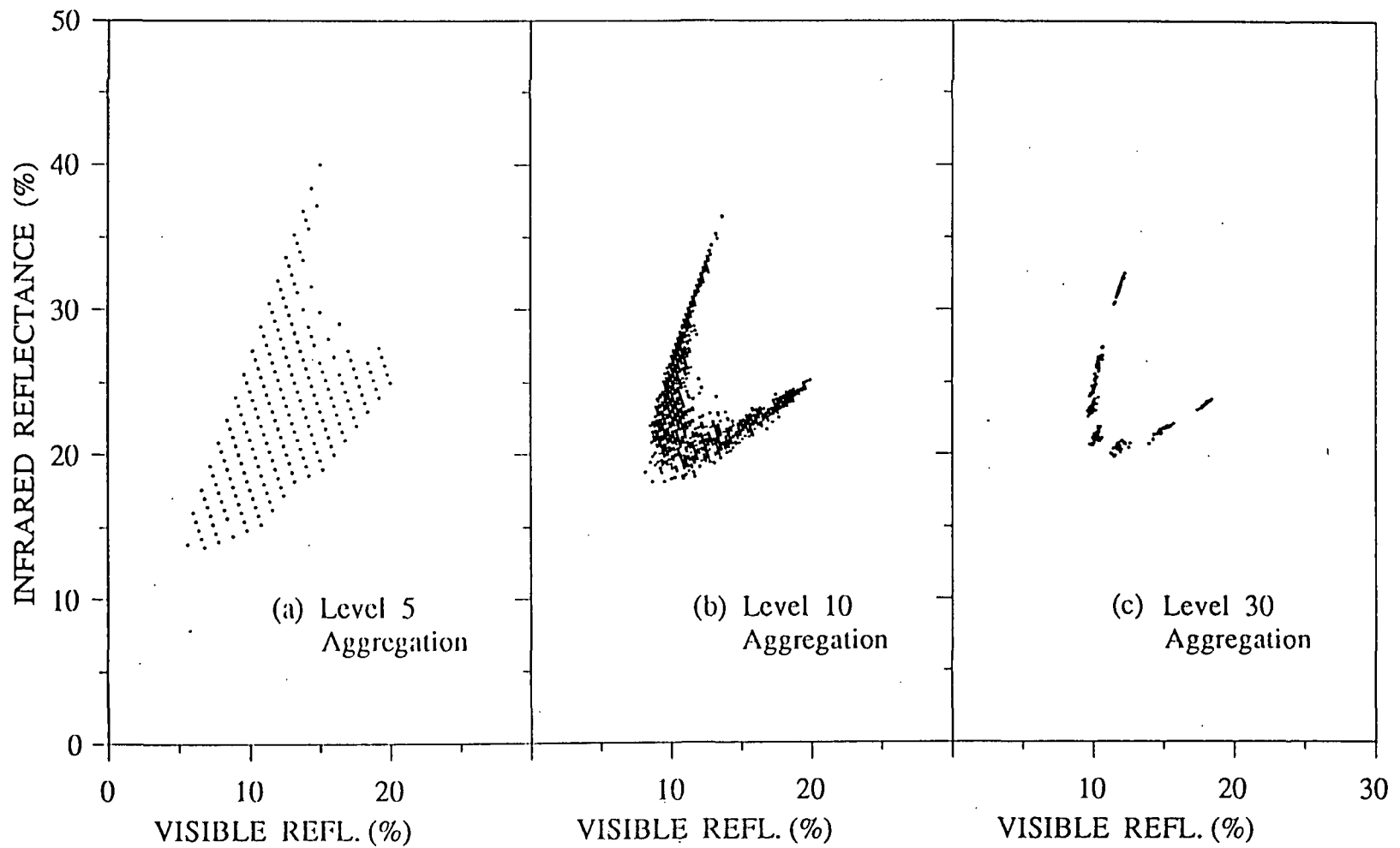


Figure 8-a,b,c. Visible-infrared scattergram, Case IV simulation: variable percent cover, constant soil and vegetation reflectances; shadowed soil background.

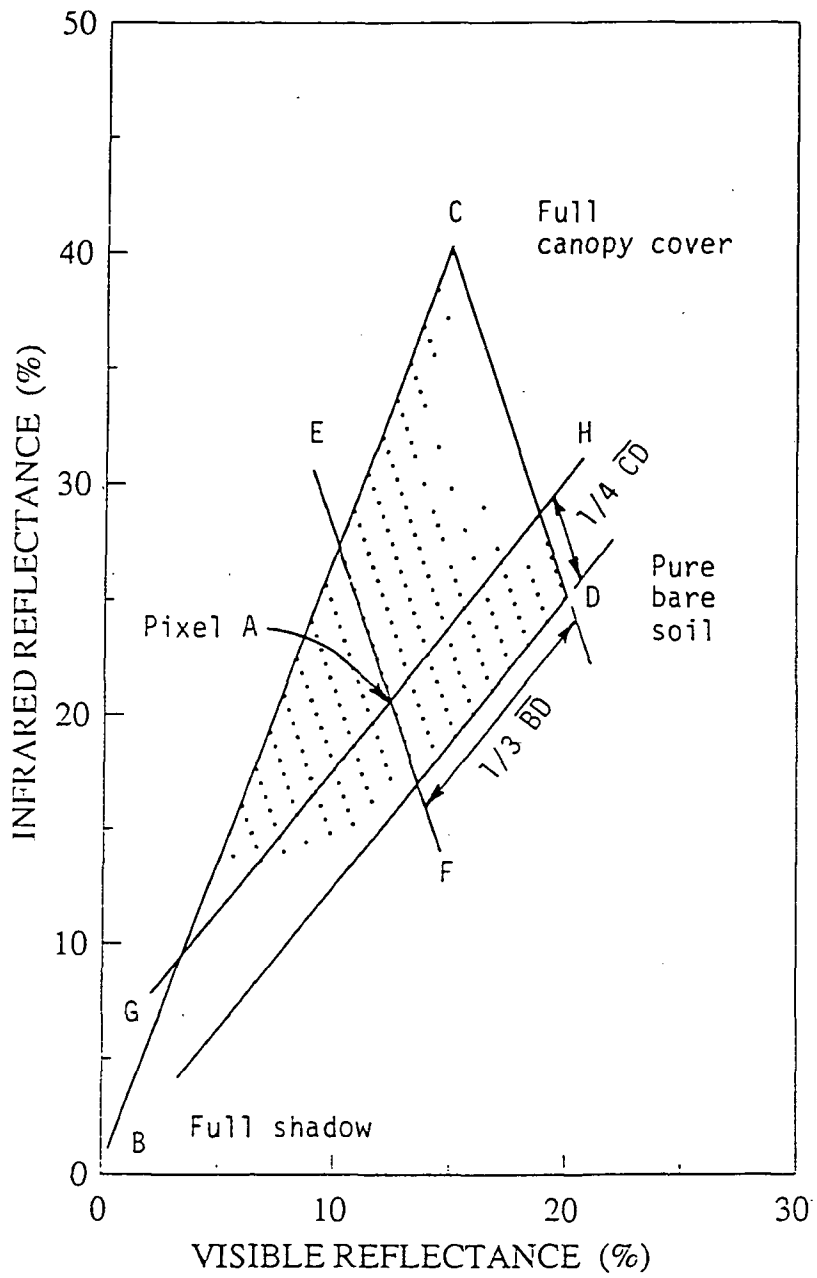


Figure 9. Interpretation of scattergram, Case IV simulation, level 5 aggregation: variable percent cover, constant soil and vegetation reflectances; shadowed soil background.

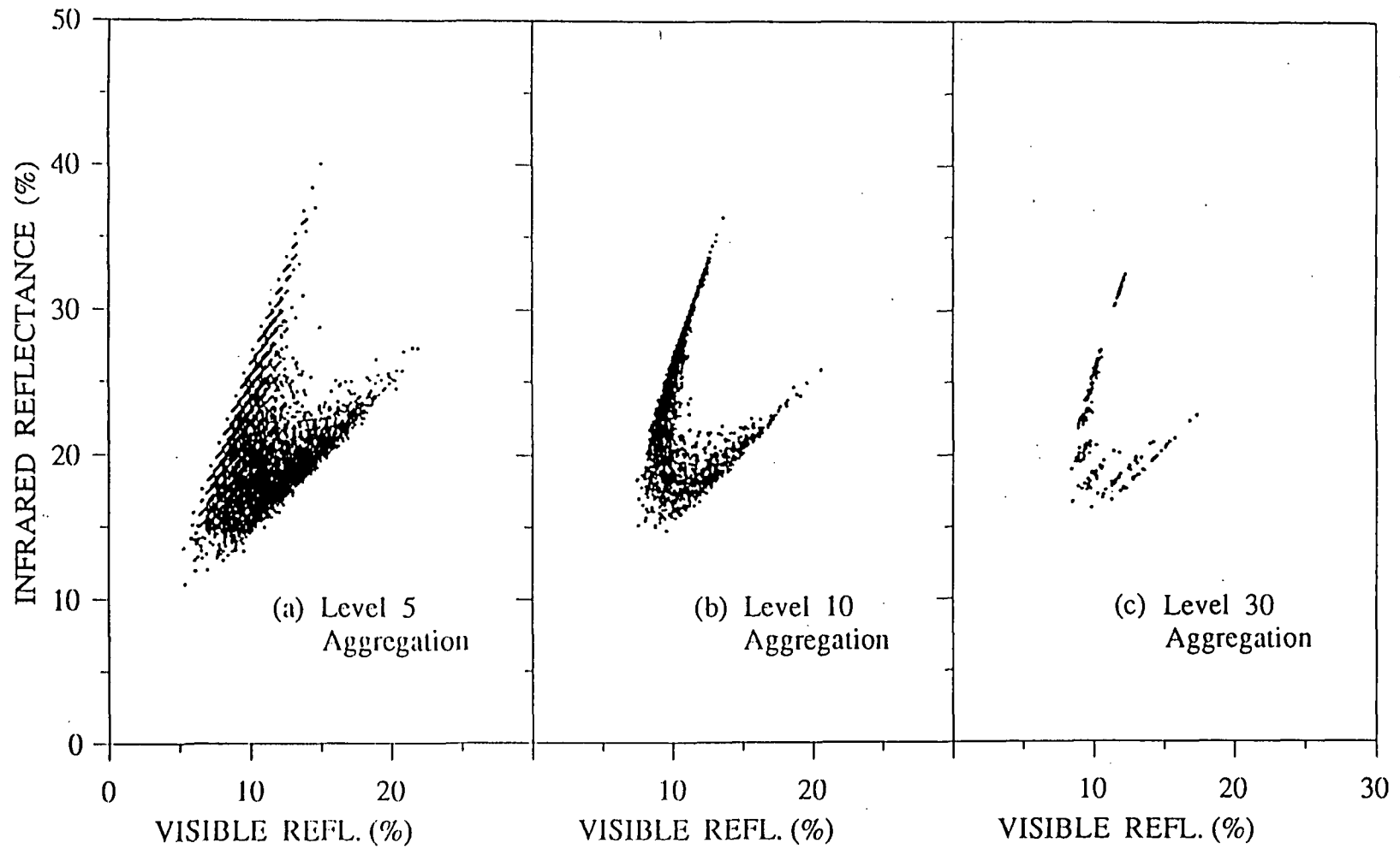


Figure 10-a,b,c. Visible-infrared scattergrams, Case V simulation: variable percent cover and soil reflectance, constant vegetation reflectance; shadowed soil background.

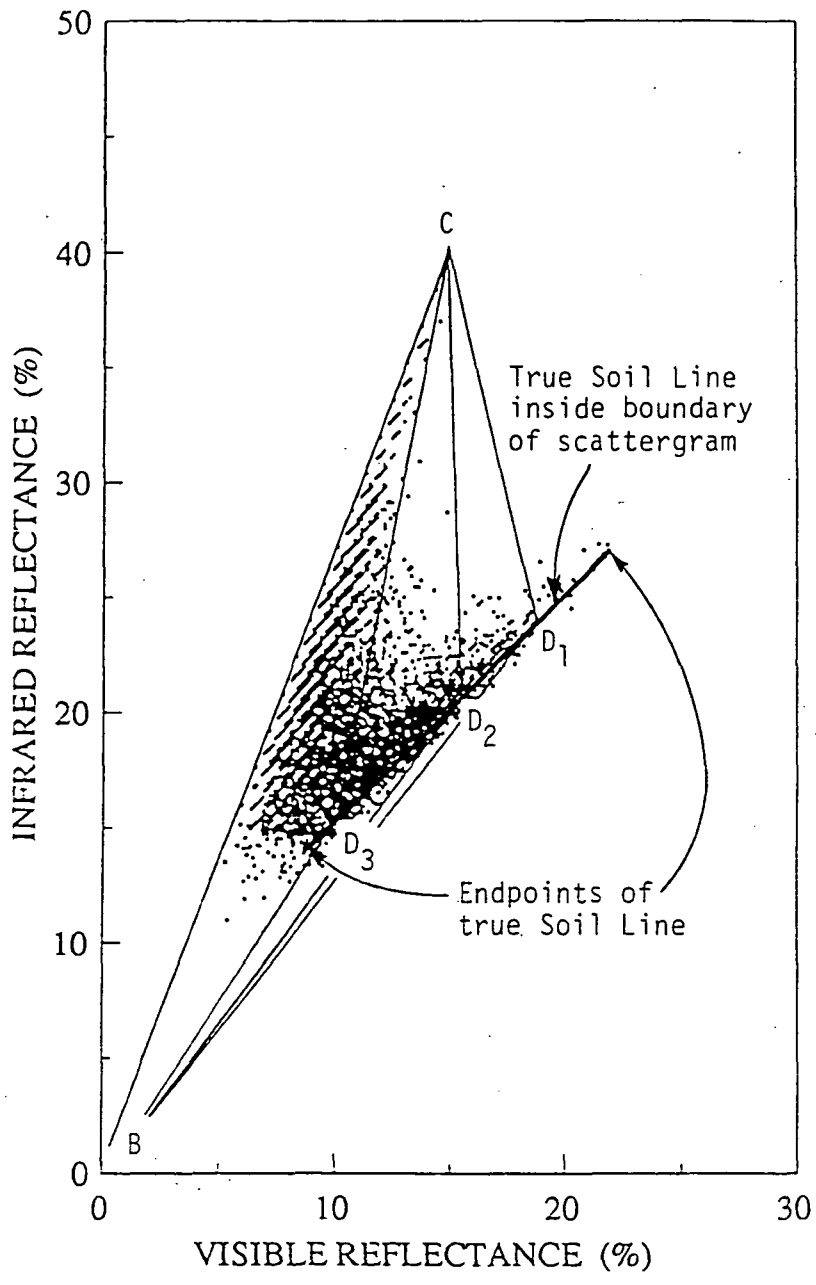


Figure 11. Interpretation of scattergram, Case V simulation, level 5 aggregation: variable percent cover and soil reflectances, constant vegetation reflectance; shadowed soil background.

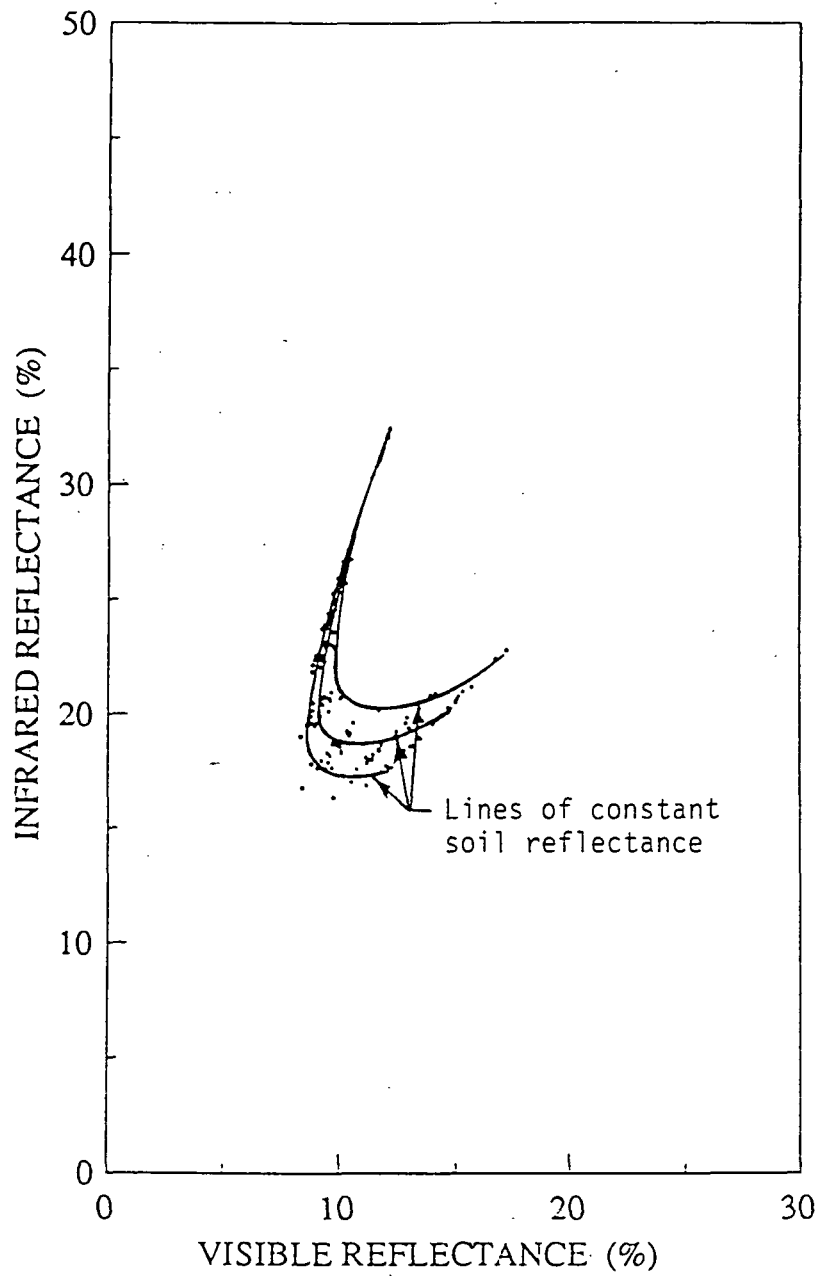


Figure 12. Interpretation of scattergram, Case V simulation, level 30 aggregation: variable percent cover and soil reflectance, constant vegetation reflectance; shadowed soil background.